


## Fast-moving target tracking by dual-geometric moment detection

Chao Shen(申超), Xu-Ri Yao(姚旭日), Fan Liu(刘璠), and Shijian Li(李世剑)
**Citation:**Chin. Phys. B, 2026, 35 (**6**): 064205. DOI: 10.1088/1674-1056/ae4c73
http://cpb.iphy.ac.cn; http://iopscience.iop.org/cpb

**What follows is a list of articles you may be interested in**

---

## Design of a compact wide-field-of-view infrared imager based on wavefront coding

Chonghui Zhu(朱崇辉), Jiaqian Yu(于佳倩), and Jingang Cui(崔金刚)
Chin. Phys. B, 2026, 35 (**2**): 024202. DOI: 10.1088/1674-1056/adf03f

## Image-free single-pixel semantic segmentation for complex scene based on multi-scale U-Net

Tengfei Liu(刘腾飞), Yanfeng Bai(白艳锋), Jianxia Chen(陈健霞), Jintao Zhai(翟锦涛), Siqing Xiang(向思卿), Xianwei Huang(黄贤伟), and Xiquan Fu(傅喜泉)‡
Chin. Phys. B, 2026, 35 (**1**): 014202. DOI: 10.1088/1674-1056/ade4b0

## Color Fourier single-pixel imaging with random color filter array

Jialiang Chen(陈佳亮), Wei Zhu(朱维), Le Wang(王乐), and Shengmei Zhao(赵生妹)
Chin. Phys. B, 2025, 34 (**9**): 094210. DOI: 10.1088/1674-1056/adf1e9

## High-quality ghost imaging based on undersampled natural-order Hadamard source

Kang Liu(刘炕), Cheng Zhou(周成), Jipeng Huang(黄继鹏), Hongwu Qin(秦宏伍), Xuan Liu(刘轩), Xinwei Li(李鑫伟), and Lijun Song(宋立军)
Chin. Phys. B, 2024, 33 (**9**): 094204. DOI: 10.1088/1674-1056/ad62e1

## Efficient single-pixel imaging encrypted transmission based on 3D Arnold transformation

Zhen-Yu Liang(梁振宇), Chao-Jin Wang(王朝瑾), Yang-Yang Wang(王阳阳), Hao-Qi Gao(高皓琪), Dong-Tao Zhu(朱东涛), Hao-Li Xu(许颢砾), and Xing Yang(杨星)
Chin. Phys. B, 2024, 33 (**3**): 034204. DOI: 10.1088/1674-1056/acf204

---

**RAPID COMMUNICATION**

# Fast-moving target tracking by dual-geometric moment detection

Chao Shen(申超)[1], Xu-Ri Yao(姚旭日)[1,2], Fan Liu(刘璠)[3,†], and Shijian Li(李世剑)[4,5,‡]

[1] *Center for Quantum Technology Research and Key Laboratory of Advanced Optoelectronic Quantum Architecture and Measurements, School of Physics, Beijing Institute of Technology, Beijing* 100081, *China*

[2] *Center for Interdisciplinary Science of Optical Quantum and NEMS Integration, School of Physics, Beijing Institute of Technology, Beijing* 100081, *China*

[3] *Key Laboratory of Electronics and Information Technology for Space Systems, National Space Science Center, Chinese Academy of Sciences, Beijing* 100190, *China*

[4] *College of Photonics and Optical Engineering, Aerospace Information Technology University, Jinan* 250299, *China*

[5] *Shandong Key Laboratory of Intelligent Photonic Transmission and Sensing, Jinan* 250299, *China*

(Received 5 February 2026; revised manuscript received 26 February 2026; accepted manuscript online 3 March 2026)

This paper presents a high-speed single-pixel tracking method that exceeds the modulation speed limit of the digital micromirror device (DMD) in conventional approaches. The proposed method adopts a polarization system to split the target image into two identical beams, which are modulated by two orthogonal steady-state geometric moment patterns and input into the dual channels of the DMD. This allows separate extraction of the target's *x*- and *y*-direction positional information without DMD pattern switching. The localization speed is no longer constrained by DMD switching but determined by high-speed single-pixel detectors. Experimental results demonstrate a localization speed of 450 kHz, achieving a one-order-of-magnitude improvement over traditional DMD-based methods.

**Keywords:** target tracking, geometric moment, single-pixel detection

**PACS:** 42.30.Va, 42.30.Ms

**DOI:** 10.1088/1674-1056/ae4c73 **CSTR:** 32038.14.CPB.ae4c73

## 1. Introduction

Moving target tracking[1–9] has broad applications across diverse fields, including aerospace,[5] biomedicine,[6–8] and industrial control.[9] Conventionally, trajectory data are acquired using imaging systems equipped with array detectors. However, these detectors — typically operating at frame rates $\leq$ 10 kfps — are inadequate for localizing high-speed targets. High-frame-rate operation further exacerbates data overload, imposing significant strain on data transmission and storage systems and rendering long-term observation impractical. Moreover, the requirement for post-processing involving inter-frame calculations hinders real-time trajectory acquisition.

Single-pixel imaging (SPI)[10–12] is a computational imaging technique that reconstructs high-resolution images using a single-pixel detector paired with a spatial light modulator (SLM). Unlike conventional imaging methods that rely on array detectors, SPI captures intensity measurements of sequentially projected patterns and employs algorithms like compressed sensing to reconstruct the scene. This approach offers advantages in low-light conditions,[13] hyperspectral imaging,[14] and non-visible wavelengths,[15–17] where traditional cameras struggle due to sensor limitations or cost constraints. However, the imaging speed of SPI is fundamentally constrained by the modulation speed, which leads to an insufficient frame rate when imaging dynamic scenes. To enable single-pixel imaging of moving targets, two primary strategies have been explored: increasing the modulation rate[18–22] and incorporating motion compensation techniques.[23–32] For example, LED illumination,[18] rotating masks,[19–21] and sweeping aggregation patterns[22] have been used to increase the modulation speed up to the MHz level. Meanwhile, motion-induced blur can be reduced using methods such as motion estimation,[23] cross-correlation,[24] two-dimensional (2D) projective patterns,[25] time-resolved SPI,[26] laterally shifted patterns,[27] four-quadrant detectors,[28] Fourier modulation,[29–31] and geometric moment-based patterns.[32] Recently, image-free moving target tracking methods based on SPI have been proposed.[33–45] Some of these methods ingeniously capitalize on the high-speed modulation functionality of the digital micromirror device (DMD), a prevalent form of SLM extensively employed in SPI, while the remaining methods use designed masks to achieve high-speed modulation. In addition, these methods fully take advantage of the high-response-frequency characteristics of single-point detectors. In 2019, Shi *et al.* used 128 Hadamard patterns to achieve real-time tracking at 177 Hz.[40] Subsequently, Fourier basis patterns were employed to achieve a temporal resolution of

†Corresponding author. E-mail: liufan@nssc.ac.cn

‡Corresponding author. E-mail: lishijian@aitech.edu.cn

© 2026 Chinese Physical Society and IOP Publishing Ltd. All rights, including for text and data mining, AI training, and similar technologies, are reserved.

1666 fps with a 10000 Hz DMD.[41] In 2021, Zha *et al.* further demonstrated that fast-moving object tracking can be achieved at 7400 Hz by measuring zero-order and first-order geometric moments.[42] Tang *et al.* achieved a single-pixel tracking rate of up to 400 kHz and a wide spectral range of visible near-infrared using a rotating mask.[43] Geometric moments are capable of achieving one-dimensional (1D) positioning by utilizing merely three frame patterns, and at present, they represent the most rapid positioning method available. In an effort to further accelerate the positioning speed, positioning strategies that capitalize on the complementary characteristics of the DMD have been put forward. In the complementary single-pixel fast-moving object tracking method proposed by Zha *et al.*, only two geometric moment patterns are required for modulation. Two identical single-pixel detectors are utilized in two specific directions corresponding to the DMD.[44] This method enables a frame rate of up to 11.1 kHz. Then, Yang *et al.* employed complementary single-pixel detection and centralized geometric moments to simultaneously achieve target localization and classification.[45]

In this paper, we propose a single-pixel moving target tracking method based on steady-state geometric moment patterns and complementary measurements. As noted previously, traditional single-pixel tracking approaches that rely on geometric moments require the projection of multiple patterns to achieve target localization. Even when a complementary measurement is implemented with a DMD, two patterns are still needed for the measurement process. Consequently, the maximum localization speed of the entire system is limited by the maximum modulation speed of the DMD, which is typically 22 kHz. Our proposed method employs a polarization system to duplicate and split the target image into two beams. These two identical images are then modulated using two orthogonal steady-state geometric moment patterns and, respectively, fed into the dual channels of the DMD. In this manner, we separately extract the positional information of the target image along the $x$- and $y$-directions, thus retrieving the two-dimensional motion information of the object. During this process, the geometric moment patterns remain static; therefore, the localization speed is no longer limited by the DMD's switching rate but instead is determined by the detection and acquisition system. Given that single-point detectors exhibit high-speed response capabilities, our experimental results demonstrate that this method can effectively achieve a localization speed of 450 kHz, which constitutes an improvement of one order of magnitude over conventional DMD-based approaches.

## 2. Method

Geometric moments provide a concise mathematical description of the spatial distribution of an object's intensity. Physically, the zero-order moment corresponds to the total integrated intensity of the object, while the first-order moments indicate the intensity-weighted centroid coordinates along the $x$ and $y$ axes. Based on this principle, geometric moment patterns are constructed by assigning position-dependent weights along a given axis, such that the detected signal corresponds to a weighted integral of the object's intensity distribution. This establishes a direct relationship between the measured signal and the object's positional coordinate along that axis. By performing measurements along two orthogonal axes, the centroid coordinates of the object can be uniquely determined. The detailed theoretical framework for centroid extraction using geometric moment patterns is presented below. For an object $O(x,y)$ in the two-dimensional (2D) space, its geometric moments are defined as follows:

$$m_{pq} = \iint_{x,y} x^p y^q O(x,y)\,\mathrm{d}x\mathrm{d}y, \tag{1}$$

where both $p$ and $q$ are non-negative integers, and $p+q$ denotes the order of the geometric moment $m_{pq}$. Based on Eq. (1), the zero-order moment $m_{00}$ and two first-order moments $m_{10}$ and $m_{01}$ of the target can be calculated. Specifically, the zero-order moment represents the total brightness of the object, while the first-order moments are correlated with the centroid coordinates of the object. Their respective expressions are given as follows:

$$m_{00} = \iint_{x,y} O(x,y)\,\mathrm{d}x\mathrm{d}y, \tag{2}$$

$$m_{10} = \iint_{x,y} x\cdot O(x,y)\,\mathrm{d}x\mathrm{d}y, \tag{3}$$

$$m_{01} = \iint_{x,y} y\cdot O(x,y)\,\mathrm{d}x\mathrm{d}y. \tag{4}$$

By utilizing the relationship between the zero-order moment and the first-order moments, the centroid position $(x_\mathrm{c}, y_\mathrm{c})$ of the target can be calculated as follows:

$$x_\mathrm{c} = \frac{m_{10}}{m_{00}}, \quad y_\mathrm{c} = \frac{m_{01}}{m_{00}}. \tag{5}$$

The specific discretized forms corresponding to $m_{00}$, $m_{10}$, and $m_{01}$ in a region of pixels $N\times N$ are expressed as follows:

$$\boldsymbol{P}_{00} = \begin{bmatrix} 1 & 1 & \cdots & 1 \\ 1 & 1 & \cdots & 1 \\ \vdots & \vdots & \ddots & \vdots \\ 1 & 1 & \cdots & 1 \end{bmatrix}, \quad \boldsymbol{P}_{10} = \begin{bmatrix} 1 & 2 & \cdots & N \\ 1 & 2 & \cdots & N \\ \vdots & \vdots & \ddots & \vdots \\ 1 & 2 & \cdots & N \end{bmatrix},$$

$$\boldsymbol{P}_{01} = \begin{bmatrix} N & N & \cdots & N \\ N-1 & N-1 & \cdots & N-1 \\ \vdots & \vdots & \ddots & \vdots \\ 1 & 1 & \cdots & 1 \end{bmatrix}. \tag{6}$$

The aforementioned grayscale geometric moment patterns $P_{00}$, $P_{10}$, and $P_{01}$ need to be binarized via Floyd–Steinberg dithering[46] after normalization, as shown in Fig. 1(a), and then loaded and displayed on the DMD. The optical signal

from the object, after modulation by the geometric moment patterns, is acquired by a single-point detector. The corresponding intensity measurements are given by

$$I_{00} = \sum_{x,y} P_{00}(x,y)O(x,y), \tag{7}$$

$$I_{10} = \sum_{x,y} P_{10}(x,y)O(x,y), \tag{8}$$

$$I_{01} = \sum_{x,y} P_{01}(x,y)O(x,y). \tag{9}$$

Thus, the centroid pixel position $(x_{Nc}, y_{Nc})$ of the object can be obtained using the following formula:

$$x_{Nc} = \frac{I_{10}}{I_{00}} \times N, \quad y_{Nc} = \frac{I_{01}}{I_{00}} \times N. \tag{10}$$

In traditional SPI tracking methods, the geometric moment patterns $P_{00}$, $P_{10}$, and $P_{01}$ are sequentially displayed on the DMD to acquire the corresponding intensity values $I_{00}$, $I_{10}$, and $I_{01}$ in order, as shown in Fig. 1(b). The centroid position of the object is then calculated based on these measurements. Therefore, the tracking speed is determined by the flipping rate of the DMD. However, in the proposed approach, $I_{00}$, which represents the total intensity of the object, is first measured or estimated using prior knowledge. Subsequently, the geometric moment patterns $P_{10}$ and $P_{01}$ are displayed simultaneously on the DMD in parallel, as shown in Fig. 1(c). After passing through the polarizing beam-splitting system, the object image is split into two identical copies, which are projected onto the regions corresponding to $P_{10}$ and $P_{01}$, respectively. As shown in Fig. 1(d), the intensities modulated by $P_{10}$ and $P_{01}$ are detected separately in the two reflected channels of the DMD, enabling the simultaneous acquisition of the object's centroid positions along the $x$- and $y$-directions. During subsequent object tracking, the parallel patterns $P_{10}$ and $P_{01}$ displayed on the DMD remain unchanged. Consequently, the tracking speed is no longer constrained by the DMD's flipping rate but is instead determined by the response speed of the detectors or the data acquisition systems.

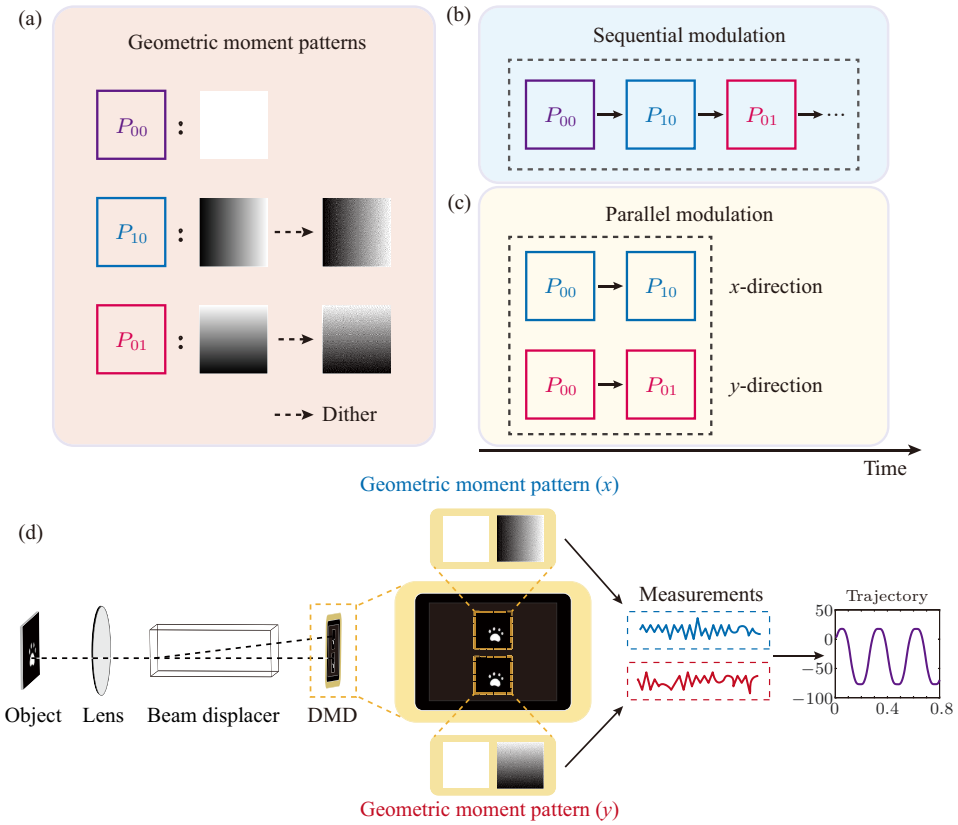



**Fig. 1.** Schematic diagram of the proposed method. (a) Geometric moment patterns used for localization. The patterns are binarized via spatial dithering. (b) Sequential modulation. Object position information is obtained through the cyclic modulation of the three patterns. (c) Parallel modulation. Each channel uses only two patterns. (d) Dual-channel parallel tracking system. The object is split into two images and imaged onto separate regions of the DMD through a lens and a beam displacer. Geometric moment patterns are projected individually along the $x$- and $y$-directions on these regions. After modulation, the signals are collected by two detectors and digitized by a data acquisition board to obtain the measurements. Finally, the trajectory of the object is obtained using the geometric moment localization algorithm.

## 3. Experimental results

We performed tracking experiments to validate the effectiveness of the proposed method. The experimental setup is schematically illustrated in Fig. 2. The DMD model employed in the experiments is the TI DLP-7000, featuring a resolution of 1024 × 768 micromirror units and a maximum mirror switching frame rate of 20 kHz. Binarized geometric moment patterns $P_{10}$ and $P_{01}$, each with a pixel size of 128 × 128, were displayed in parallel on the DMD. Light

from the object was split into two beams by a calcite system (Thorlabs BD40), which were then imaged separately onto the regions corresponding to $P_{10}$ and $P_{01}$. Two photomultiplier tubes (PMTs, Hamamatsu H15460-40-01) with semicircular diaphragms were independently positioned in the two reflection channels of the DMD — corresponding to angular orientations $+12^\circ$ (channel 1) and $-12^\circ$ (channel 0) — to function as point detectors. The two beams emerging from the calcite system are linearly polarized with mutually perpendicular polarization directions. Linear polarizers aligned with the respective polarization directions of the two beams were placed in front of the two detectors. This configuration enables the isolation of the reflected light from regions $P_{10}$ and $P_{01}$, allowing the detectors to separately measure the modulated reflected light from each region. The signals from the two detectors were processed using a data acquisition system (DAQ; National Instruments, USB-6361). The maximum frequency bandwidth of the PMT is 30 MHz, while the maximum sampling rate of the dual-channel DAQ is 1 MS/s; thus, the speed of the measurement system is ultimately determined by the sampling rate of the DAQ.

First, we performed a positioning experiment on a rotating moving target. The object is a 2-cm-diameter circular white card, which is driven by a motor to move along a 5.4-cm-diameter circular trajectory at 88 r/min, and is illuminated by an annular light-emitting diode (LED; MV-LRDS-H-160-60-W2). The sampling rate of the dual-channel DAQ used in this experiment was 200 kS/s. The object motion curve recovered by the proposed method is shown in Fig. 3(a). Figures 3(b) and 3(c) show the $x$-axis and $y$-axis positions of the object obtained using the proposed method and the conventional sequence modulation method within a 1 ms measurement interval. It can be seen that the proposed method can achieve 200 samplings within this time interval, which is much more than the 6 samplings provided by the conventional method.

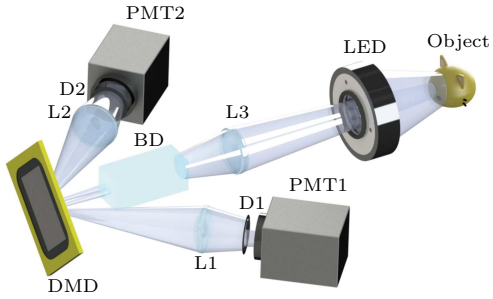



**Fig. 2.** Experimental setup of the dual-channel localization system. The object is illuminated by an annular light-emitting diode (LED). The reflected light is split into two orthogonally polarized beams due to the birefringence effect of the calcite crystal in the beam displacer (BD). Subsequently, the two beams are imaged onto two separate regions of the DMD. After being modulated by the DMD, the beams reflected at $\pm 12^\circ$ are guided into two detection paths, each containing a linear polarizer aligned with the respective polarization direction to isolate the corresponding beam and minimize cross-talk. Semicircular diaphragms are inserted in the detection paths to further separate the beams and reduce interference. Finally, the signals are independently detected by two identical PMTs and converted into measurements via the data acquisition system. L: lens, $f_1 = f_2 = 4$ cm, $f_3 = 15$ cm; BD: beam displacer; D: diaphragm.

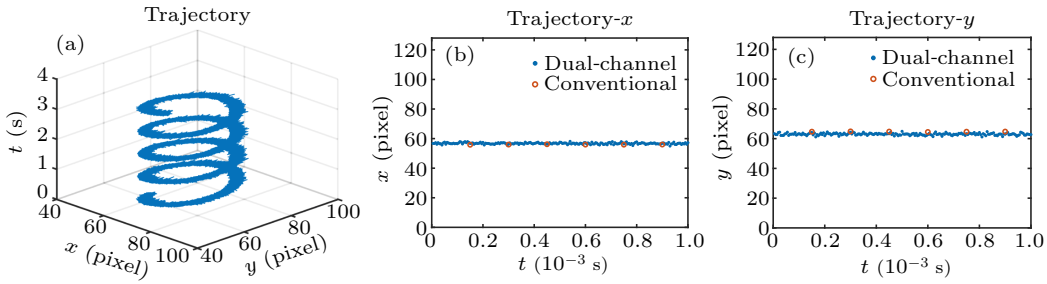



**Fig. 3.** Positioning results of the rotating object. (a) 3D trajectory obtained by the dual-channel method at a tracking frequency of 200 kHz. Positioning results for (b) the $x$-axis and (c) the $y$-axis obtained by two methods.

To further verify the high-speed positioning ability of our method, we conducted experiments to locate high-speed time-varying point targets generated by a projection system. In this experiment, five points flashed sequentially along a straight line, which were generated by an external projection system. The system used a DLP-6500 DMD device that operated at its maximum switching frequency of 9 kHz during the experiment. Two sampling rates (100 kS/s and 450 kS/s) of the dual-channel DAQ were used. The tracking results are illustrated in Fig. 4. The dual-channel positioning method can accurately reconstruct the five sequential flashing points. As illustrated in Figs. 4(a), 4(b) and 4(d), 4(e), since the sampling rate of the measurement and acquisition system is much higher than the maximum frame rate of the DLP projection system, each flashed point is sampled multiple times. As observed in Figs. 4(d) and 4(e), several offset points appear around the five target points. These offsets are mainly caused by the fact that DMD micromirrors require approximately 8 μs to reach a steady state during switching; during this period, the light intensity fluctuates, which affects the positioning accuracy. As shown in Figs. 4(c) and 4(f), restricted by its positioning frequency, the conventional single-channel geometric moment method yields only one positioning point at a DMD operating frequency of 9 kHz (corresponding to a positioning frequency of 3000 Hz) and merely three positioning points even at the maximum DMD switching frequency of 20 kHz (corresponding to a positioning frequency of 6666 Hz), thus making it entirely incapable of resolving and positioning all five points.

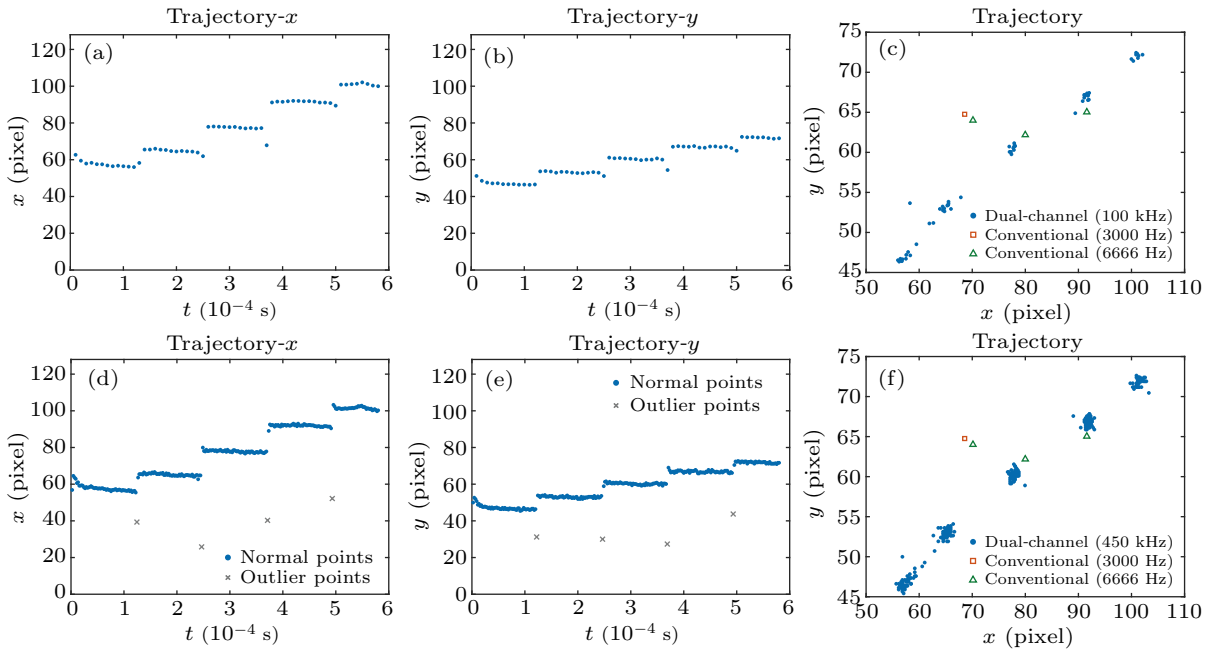



**Fig. 4.** Positioning results of high-speed time-varying point target. The $x$-axis trajectory, $y$-axis trajectory, and 2D trajectory obtained by the proposed dual-channel method at a sampling rate of 100 kHz are shown in (a), (b), and (c), respectively. For comparison, results from the conventional method at sampling rates of 3000 Hz and 6666 Hz are also plotted in (c). The results of the proposed dual-channel method at a sampling rate of 450 kHz are shown in (d), (e), and (f), respectively, where outliers for the dual-channel method have been removed in (f).

## 4. Discussion and conclusion

Compared with existing methods, the proposed method employs polarization splitting and parallel geometric-moment patterns to modulate the light field. This design avoids the need for DMD-based pattern flipping and provides advantages in tracking rate. Static patterns do not introduce inherent limits on modulation speed, so the tracking rate is mainly limited by the data acquisition speed of the single-pixel detector. In our hardware implementation, the maximum acquisition rate reaches 450 kHz. By comparison, DMD-based tracking methods are limited by the DMD switching rate, which is typically about 22 kHz. Although the feasibility of the system has been experimentally verified, the current system relies on polarization beam splitting and requires the target response to remain consistent across polarization channels. Polarization-insensitive beam-splitting schemes could be investigated to further improve system robustness.

In summary, a high-speed single-pixel tracking method that combines polarization splitting technology with steady-state geometric moment modulation is proposed, offering a novel solution to overcome the DMD modulation speed limit in traditional SPI tracking systems. Comprehensive experimental results validate the effectiveness and superiority of the proposed method, demonstrating that it can achieve a localization speed of 450 kHz — one order of magnitude higher than that of conventional DMD-modulation-limited approaches. In subsequent work, GHz-range positioning performance can be realized by combining high-speed fiber optic detectors with oscilloscopes. With its advantages of high localization speed, high precision, and simple system configuration, this method has broad application prospects in fields such as high-speed dynamic target detection, industrial monitoring, and biomedical imaging.

## Data availability statement

The data underlying the results presented in this paper are not publicly available at this time but may be obtained from the authors upon reasonable request.

## Acknowledgements

This work was supported by the National Natural Science Foundation of China (Grant No. 12504337) and Beijing Institute of Technology Research Fund Program for Young Scholars (Grant No. 202122012).

## References

[1] Gariepy G, Tonolini F, Henderson R, Leach J and Faccio D 2016 *Nat. Photonics* **10** 23
[2] Wei M S, Xing F and You Z 2018 *Light: Sci. Appl.* **7** 18006
[3] Sun N Y, Zhao J, Shi Q, Liu C and Liu P 2024 *IEEE Trans. Ind. Informat.* **20** 7056
[4] Yan B B, Wei Y X, Liu S X, Huang W, Feng R Z and Chen X Q 2025 *Def. Technol.* **51** 201
[5] Li X R and Jilkov V P 2003 *IEEE Trans. Aerosp. Electron. Syst.* **39** 1333
[6] Smal I, Draegestein K, Galjart N, Niessen W and Meijering E 2008 *IEEE Trans. Med. Imag.* **27** 789
[7] Rohr K, Godinez W J, Harder N, Wörz S, Mattes J, Tvaruskó W and Eils R 2010 *Cold Spring Harb. Protoc.* **6** pdb.top80
[8] Maška M, Ulman V, Svoboda D, *et al.* 2014 *Bioinformatics* **30** 1609
[9] Liu G P 2023 *IEEE/CAA J. Autom. Sinica* **10** 216

[10] Sun B, Edgar M P, Bowman R, Vittert L E, Welsh S, Bowman A and Padgett M J 2013 *Science* **340** 844
[11] Edgar M P, Gibson G M and Padgett M J 2019 *Nat. Photonics* **13** 13
[12] Gibson G M, Johnson S D and Padgett M J 2020 *Opt. Express* **28** 28190
[13] Liu S, Chen B, Zou W Z, Sha H, Feng X C, Han S Y, Li X, Yao X R, Zhang J and Zhang Y B 2024 *Commun. Eng.* **3** 88
[14] Meng H Y, Gao Y, Wang X H, Li X Y, Wang L L, Zhao X and Sun B Q 2024 *Light: Sci. Appl.* **13** 121
[15] Stantchev R I, Yu X, Blu T and Pickwell-MacPherson E 2020 *Nat. Commun.* **11** 2535
[16] Li W L, Hu X M, Wu J B, Fan K B, Chen B W, Zhang C H, Hu W, Cao X, Jin B B, Lu Y Q, Chen J and Wu P H 2022 *Light: Sci. Appl.* **11** 191
[17] Wang Y Q, Huang K, Fang J N, Yan M, Wu E and Zeng H P 2023 *Nat. Commun.* **14** 1073
[18] Xu Z H, Chen W, Penuelas J, Padgett M and Sun M J 2018 *Opt. Express* **26** 2427
[19] Jiang W, Jiao J, Guo Y, Chen B, Wang Y and Sun B 2021 *Opt. Lett.* **46** 4859
[20] Hahamovich E, Monin S, Hazan Y and Rosenthal A 2021 *Nat. Commun.* **12** 4516
[21] Zhao Z Q, Zhang Y X, Song J Q, Li M F and Wu L A 2025 *Opt. Lett.* **50** 169
[22] Kilcullen P, Ozaki T and Liang J 2022 *Nat. Commun.* **13** 7879
[23] Jiao S, Sun M, Gao Y, Lei T, Xie Z and Yuan X 2019 *Opt. Express* **27** 12841
[24] Wu J, Hu L and Wang J 2021 *Opt. Express* **29** 42589
[25] Yang W, Shi D, Han K, Guo Z, Chen Y, Huang J, Ling H and Wang Y 2022 *Opt. Lett.* **47** 3123
[26] Jiang W, Yin Y, Jiao J, Zhao X and Sun B 2022 *Photon. Res.* **10** 2157
[27] Sun S, Hu H K, Xu Y K, Li Y G, Lin H Z and Liu W T 2022 *Phys. Rev. Appl.* **17** 024050
[28] Du L K, Sun S, Jiang L, Chang C, Lin H Z and Liu W T 2023 *Phys. Rev. Appl.* **19** 054014
[29] Li S, Yao X R, Zhang W, Wang Y and Zhao Q 2024 *Phys. Rev. Appl.* **22** 044007
[30] Yu Y, Yang Z H, Ji P C, Li M F, Wu L A and Yu Y J 2025 *IEEE Trans. Instrum. Meas.* **74** 4513209
[31] Hu J, Chen K, Min L and Guo Y 2026 *Opt. Express* **34** 2433
[32] Guo Z, Shi D and Wang Y 2026 *Opt. Express* **34** 5558
[33] Yang Z H, Chen X, Zhao Z H, Song M Y, Liu Y, Zhao Z D, Lei H D, Yu Y J and Wu L A 2022 *Opt. Express* **30** 864
[34] Ji P C, Wang Y C, Zhang H J, Yang Z H and Yu Y J 2025 *Opt. Express* **33** 44497
[35] Zhang X, Xiong J, Fu A, Mok C H, Ye Z and Liu H C 2026 *Opt. Express* **34** 5028
[36] Zhang Y, Wang H J, Yin Y K, Jiang W J and Sun B Q 2023 *Opt. Express* **31** 32554
[37] Zhang H, Liu Z H, Zhou M, Zhang Z B, Chen M K and Geng Z H 2024 *Opt. Lett.* **49** 3628
[38] Guo Z J, Meng W W, Shi D F, Zha L B, Yang W, Huang J, Chen Y F and Wang Y J 2025 *Opt. Commun.* **583** 131771
[39] Peng Y C, Yang J N, Feng Y H, Yu S J, Xing F and Sun T 2025 *Sens.* **25** 3879
[40] Shi D F, Yin K X, Huang J, Yuan K, Zhu W Y, Xie C B, Liu D and Wang Y J 2019 *Opt. Commun.* **440** 155
[41] Zhang Z B, Ye J Q, Deng Q W and Zhong J G 2019 *Opt. Express* **27** 35394
[42] Zha L B, Shi D F, Huang J, Yuan K, Meng W W, Yang W, Jiang R B, Chen Y F and Wang Y J 2021 *Opt. Express* **29** 30327
[43] Tang X, Chen Z D, Chen F F, Liu C M, Pan J Y, Zhang Z B, Wu Z J, and Zhang Q C 2025 *Opt. Lett.* **50** 1469
[44] Zha L B, Meng W W, Shi D F, Huang J, Yuan K, Yang W, Chen Y F and Wang Y J 2022 *Opt. Lett.* **47** 870
[45] Yang J N , Liu X Y, Zhang L Y, Zhang L, Yan T K, Fu S, Sun T, Zhan H Y, Xing F and You Z 2025 *Opt. Express* **33** 11301
[46] Floyd R W and Steinberg L 1976 *Proc. Soc. Inf. Disp.* **17** 75